*IOSR Journal of Mechanical and Civil Engineering (IOSR-JMCE)*
*e-ISSN: 2278-1684,p-ISSN: 2320-334X, Volume 13, Issue 6 Ver. III (Nov. - Dec. 2016), PP 10-17*
*www.iosrjournals.org*

# Infrared Thermography Applied to the Prediction of Structural Vibration Behaviour

Stephen M. Talai[1], Dr. Dawood A. Desai[1], Prof. P. Stephan Heyns[2]
[1](*Department of Mechanical Engineering, Tshwane University of Technology, South Africa)*
[2](*Department Mechanical and Aeronautical Engineering, University of Pretoria, South Africa)*

***Abstract:*** *This paper concerns the development of a methodology for use of Infrared thermography (IRT) for online prediction of mechanical structural vibration behaviour; given that it has extensively been applied in non-destructive technique for evaluation of surface cracks through the observation of thermal imaging of the vibration-induced crack heat generation. To achieve this, AISI 304 steel cantilever beam coupled with a slipping friction rod subjected to a forced mechanical excitation with an infrared camera capturing the thermal profile at the friction interface. The analysed frictional temperature time-domain waveform using a MATLAB FFT algorithm and the heat conduction equation in conjunction with a finite difference approach successfully identified the structural vibration behaviour in terms of frequency and displacement, the maximum relative errors being 0.09 % and 5.85 % for frequencies and displacements, respectively. These findings are particularly useful in overcoming many limitations inherent in some of the current vibration measuring techniques in harsh and remote environments.*

***Keywords:*** *frictional heat generation, structural defect, structural health indicators, SHM, vibration*

## I. Introduction

The structural health of mechanical dynamic structures is paramount to its successful operation [1-3]. According to the past research work, the condition monitoring of vibrating structures has long been an active area of research since the 1950s; when Arthur Crawford first acknowledged the challenge to acquire an effective way for structural vibration analysis. Le et al. [4] contend that in today's mechanical and aerospace engineering communities, need for enhanced ability to monitor dynamic structures and detect the potential damages at the earliest possible stage for effective structural health monitoring (SHM) is ever increasing. For decades, however, vibration monitoring has been utilised to assess SHM in predicting potential failures that, in turn, enhance the reliability and availability [2, 5]. The direct methods of measurements such as strain gauges have predominantly been used. Although they have the advantage of performing measurement of an individual structure, it has several disadvantages such as; shorter sensor life span due to continued cyclic loading; leading to failure by fatigue [6]. Laser Doppler vibrometry with a Eulerian approach allows overcoming most of the limitations mentioned in the use of strain gauges. Nevertheless, Castellini et al. [7] reported that its main limitations are speckle effects and poor signal-to-noise ratio when measuring vibration on the low diffusive surface. Likewise, Interferometry method has the ability to provide traceability of vibration frequency measurement as it relates directly to the definition of the meter. Its measurement accuracy, however, is limited by the environment [8], thus, not be possible to perform the vibration measurement in a turbulent environment for instance power plants. Interestingly, infrared thermography (IRT) has been greatly applied to the vibrothermography non-destructive technique where the surface cracks are evaluated through the observation of thermal imaging of vibration-induced heat generation. Recent studies have shown that defect heating in cracked metallic structure is primarily generated by frictional rubbing on crack faces [9]. Mabrouki et al. [10] investigated the vibrothermography for detection of fatigue cracks in steel compact tension specimen. Lahiri et al. [11] proposed the active IRT-based technique for detecting defects in ferromagnetic specimens using low frequency alternating magnetic field induced heating. The authors observed an increase in the surface temperature using an infrared camera due to induced eddy current leading to joules heating. Furthermore, Montanini and Freni [12] established that there exists a correlation of vibrational mode shape to viscoelastic heat generation in vibrothermography.

Conversely, friction is often considered by engineers as detrimental to the design of dynamic mechanisms involving mating parts. However, it has long been established that it can as well provide a very effective means of dissipating vibratory energy in elastic structures. This technique is in applications such as turbomachinery bladed disks [2, 13], where either the lacing wire is incorporated at the chosen location of the blade structure or direct interaction of the constitutive blades through shrouded tip approach for enhancing passive dissipation of vibratory energy. In reality, it is often structural joints that are more responsible for energy dissipation than the (solid) material itself [14, 15]. Ultimately, this leads to temperature increase at the contact interface [16]. Hence, analysis of frictional heat generation acquired using IRT-based technique due to interacting components can result to a quick and reliable indication of the structural vibration behaviour.

A typical industrial application of IRT-based condition monitoring on a dynamic mechanical component *(compressor motor)* including its thermal image is presented in Fig. 1, where the abnormal surface temperature is an indication of a probable flaw. Accordingly, despite a large amount of research conducted on condition monitoring using IRT as indicated in the recent comprehensive literature review by Bagavathiappan et al. [17], little attention has been paid to vibration prediction. Interestingly, Dimarogonas and Syrimbeis [18] successfully studied the vibration modes from the thermal signature of a vibrating plate due to material damping. To date, however, the concept has not been explored even though IRT has matured and widely accepted as a condition monitoring tool where the temperature is measured in a non-contact manner.

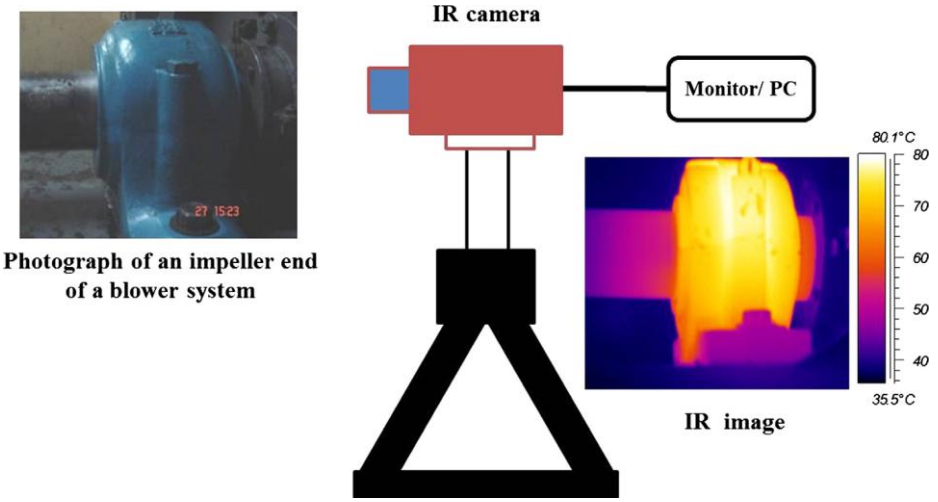


**Figure 1:** A typical practical setup for IRT based condition monitoring [17].

Consequently, it is important to mention that friction is a complex phenomenon due to its nonlinearity [19]. The difficulty, however, lies in relating frictional temperature time domain waveform to vibration behaviour. Therefore, it was the aim of this study to develop a practical methodology. In order to achieve this, AISI 304 cantilever beam coupled with slipping friction rod subjected to a forced excitation with an infrared camera capturing the thermal profile at the friction interface concurrently. An electrodynamic shaker attached to the beam end vie stinger provided the required mechanical excitation. Also, an accelerometer was attached to the beam for acquiring the actual beam displacement for the intention of validating the parameters predicted using IRT. The methodology developed forms the basis for online SHM employing IRT which is of great beneficial to the maintenance, most importantly, in harsh and turbulent environment applications.

## II. Mathematical models

### 2.1 Vibration frequencies

The post analysis of thermal imaging data yields the temperature time-domain waveform. It does not seem, by eye, to have any underlying sinusoidal signal components, instead, it seems completely random and consisting of noise. However, the Discrete Fourier Transform (DFT) analysis is utilised to check for the spectral peak. The DFT for a sequence, $x(nT)$, is given by

$$X(kF) = \sum_{n=0}^{N-1} x(nT)\, e^{-j2\pi Fnt} \qquad (1)$$

where $N$ is the number of samples, $F$ is the spacing of frequency domain samples, $T$ is the sample period in the time domain, $k$ and $n$ are integers. The MATLAB Fast Fourier Transform (FFT) function performs the computation of DFT in an efficient way. Therefore, considering the sampling frequency of an IR camera being used for SHM, and the frictional temperature time-domain waveform sequence as $X$; a Matlab FFT algorithm developed as follows:

```
Fs = f;                % sampling frequency (Hz): rated IR camera optical resolution
T = 1/Fs;              % sampling period
L = length(X);         % length of the temperature time history
Y = fft(X);
P2 = abs(Y/L);
P1 = P2(1:L/2 + 1);
```

$P1(2:end-1) = 2*P1(2:end-1);$ % FFT amplitude
$f = F_s*(0:(L/2))/L;$ % frequency range
$Plot(f, P1);$ % plots amplitude against frequency

**2.2 Correlation of beam transverse displacement to interface surface frictional temperature distribution**

The heat conduction equation for a Cartesian co-ordinate system (*x, y, z*) on the beam surface differential element can be expressed as [20]

$$\frac{\partial^2\theta}{\partial x^2}+\frac{\partial^2\theta}{\partial y^2}+\frac{\partial^2\theta}{\partial z^2}+\frac{q_g}{k}=\frac{\rho c}{k}\frac{\partial\theta}{\partial t} \quad (2)$$

where $\theta$ is the temperature rise on the beam surface, $k$ is thermal conductivity, ρ is the material density and $c$ is the specific heat capacity and $q_g$ is the heat generated per unit volume. The grid distribution technique as given in Fig. 2 analyses the surface temperature. Making the following assumptions:

1. Temperature has reached a steady state condition.
2. The beam is thin, hence the temperature distribution is uniform along the thickness.
3. Heat lost through forced convection was 30 $W/m^2.K$ at 22 °C [21]. It obeys the Newton's law of cooling ($q = h_{con}\,\theta$) and is the heat lost on both sides of the beam. However, heat loss by radiation is ignored since it's negligible compared to the heat lost through forced convection [18].

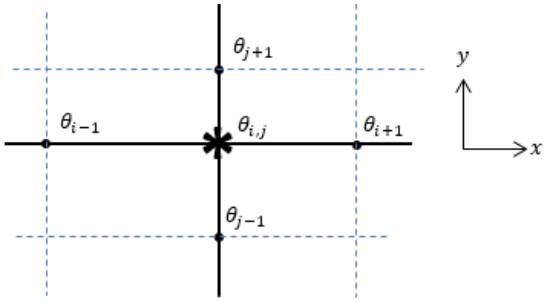


**Figure 2:** Finite surface temperature distribution grid.

Thus, the temperature rise finite difference equations for the grid in $\Delta x$ and $\Delta y$ are

$$\frac{\partial^2\theta}{\partial x^2}=\frac{1}{(\Delta x)^2}\left(\theta_{i+1}-2\theta_{i,j}+\theta_{i-1}\right), \qquad \frac{\partial^2\theta}{\partial y^2}=\frac{1}{(\Delta y)^2}\left(\theta_{j+1}-2\theta_{i,j}+\theta_{j-1}\right) \quad (3)$$

Substituting equation (3) into (2), the heat distribution in terms of temperature finite differences developed

$$q_g(x,y)=k\left[\frac{2h_{con}}{ck}\theta_{i,j}-\frac{\partial^2\theta}{\partial x^2}-\frac{\partial^2\theta}{\partial y^2}\right] \quad (4)$$

Considering a sinusoidal force for the beam excitation, the steady state displacement response can be given by [22]

$$z(t)=Z\sin(\omega t) \quad (5)$$

where z($t$) is the displacement at time $t$, $Z$ is the amplitude and $\omega$ is the excitation frequency. The frictional heat generation, $q_g$ per half a cycle, is given by [19]

$$q_g=2\mu F_{CR} f Z \quad (6)$$

where $\mu$ the coefficient of friction, $F_{CR}$ is the contact resultant force, $f$ excitation frequency, hence, substituting equation (5) into (6)

$$q_g=\frac{2\mu F_{CR} f z(t)}{\sin(\omega t)} \quad (7)$$

In order to obtain the beam displacement equation from the acquired thermal image, the surface temperature is equated to the frictional heat evaluation. Thus, comparing equation (4) and (7), the equation of beam transverse displacement is developed

$$z(t)=\frac{k\sin(\omega t-\phi)}{2\mu F_{CR}\,\omega}\left[\frac{2h_{con}}{ck}\theta_{i,j}-\frac{\partial^2\theta}{\partial x^2}-\frac{\partial^2\theta}{\partial y^2}\right] \quad (8)$$

Equation (8) allows the computation of the beam transverse displacement from the analysis of the thermal imager interface surface frictional temperature distribution.

## III. Materials and experimental method

### 3.1 Materials

Both the beam and the friction rod were manufactured of AISI 304 stainless steel due to its low thermal conductivity, hence, generate heat with slight frictional effect [10]. The geometric and material properties are given in Table 1 and Table 2, respectively.

**Table 1.**Beam and friction rod geometric dimensions.

| Description | Parameters |
|---|---|
| Beam mass | 0.10 *kg* |
| Length | 300 *mm* |
| Width | 25 *mm* |
| Thickness | 2 *mm* |
| Lacing wire diameter | 5 *mm* |
| Beam hole diameter (tolerance grade: *F8/js7*) [23] | $5^{+0.422}_{+0.412}$ *mm* |
| Beam-lacing wire hole location from fixed end | 250 *mm* |
| Exciters location from fixed end | 290 *mm* |

**Table 2.** AISI 304 material properties [24]

| *Structural properties* | Parameters |
|---|---|
| Density, $\rho$ | 7740 $kg/m^3$ |
| Young modulus, $E$ | 200 *GPa* |
| Poisson ratio, $v$ | 0.33 |
| Static friction coefficient, $\mu_s(\mu_k = 0.75\ \mu_s)$ [25] | 0.15 |
| *Thermal properties* | |
| Thermal conductivity, $k$ | 16.5 *W/m.K* |
| Specific heat capacity, $c$ | 500 *J/kg.K* |

### 3.2 Experimental Procedure

The laboratory experimental setup was as presented in Fig. 3. Initially, the pre-load force of 2.25 *N* was applied to the friction rod for the purpose of uniformity. This was achieved by tightening of the adjusting bolt that pushed the friction rod laterally via a sleeve, while a PCB force transducer model 208C02 with a sensitivity rating of 11.24 *mV/N* measured the attained force. The forcing frequency signals obtained from the function generator (FG-7005C) were amplified *(power amplifier model: LA-1500)* before being transmitted to the electrodynamic exciter *(Type: 4824, Brüel & Kjær)* to facilitate the beam mechanical forced excitation via a stinger coupled with a PCB force transducer model 208C04 with sensitivity rating of 1.124 *mV/N*, hence, measure the output force. The excitation frequencies considered were 20.0 *Hz* and 50.0 *Hz*. These were considered based on Shannon's sampling rate theorem of 0.42 times the rated optical resolution of the IR camera used in this study. Concurrently, a Micro-epsilon (TIM160) infrared camera focused on the beam-friction rod interface to capture the thermal image. This camera has a thermal sensitivity of 0.08 *K*, the spectral range of 7.5 - 13 $\mu m$, optical resolution of 160 × 120 pixels and frame rate real-time of 120 *Hz*.

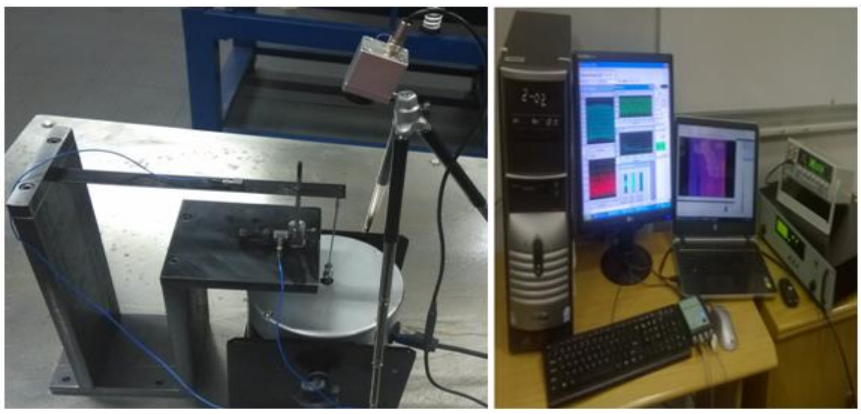

*(a)*

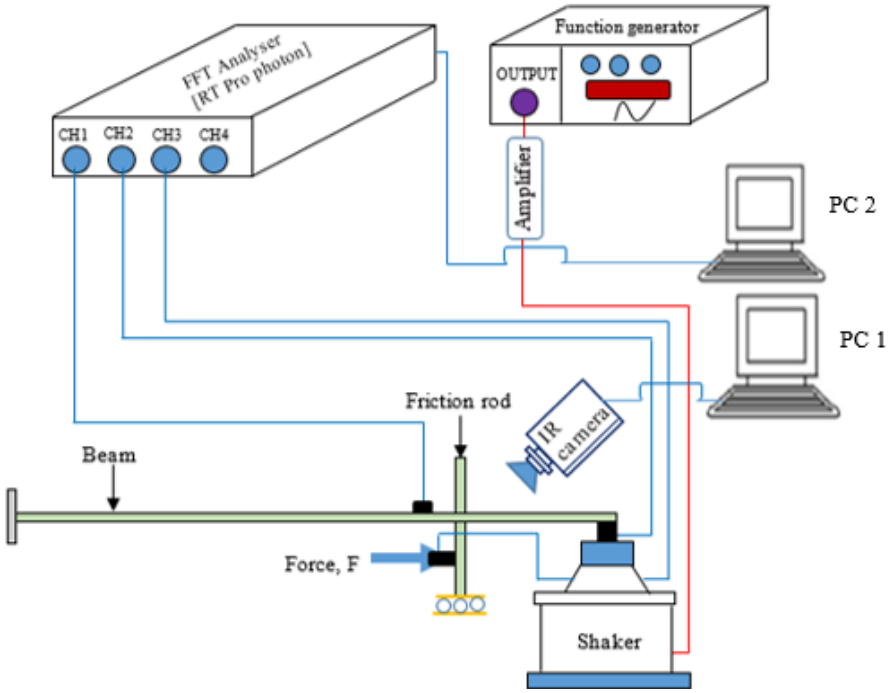


*(b)*

**Figure 3:** Frictional temperature evolution monitoring *(a) Laboratory experimental setup (b) schematic representation.*

The beam displacement response was measured using a miniature Deltatron accelerometer type 4507 with a sensitivity rating of 97.96 *mV/g* and mass of 4.8 *g* (Brüel & Kjær) that was firmly mounted to the surface. On the other hand, the RT pro-Photon FFT analyser (*Brüel & Kjær*) acquired the dynamic measurements. The problem of low thermal emissivity of the beam surface was eliminated by applying black paint which is consistent with standard practice in this field [10].

## IV. Results and discussion

The analysis presented comprises of beam forcing frequencies of 20.0 *Hz* and 50.0 *Hz*. During this particular period, the ambient room temperatures recorded was 22.4 °C. The thermal imaging considered 150 *s* recording time as required by the operation manual for the reliable real-time temperature recording *(full pixel recording).* This short time duration went a long way in avoiding the effect of significant wear rate at friction interface during excitation. The acquired images with the grid interface temperature distributions emanating from these frequencies were as shown in Fig. 4, while the frictional temperature evolution time-domain waveform corresponding to the hottest interface in Fig. 5. As expected, the structure under higher excitation frequency allows the frictional interface to slide against each other more time; unlike at lower frequencies leading to greater frictional heat generation as seen with a temperature difference of 1.2 °C among the images.

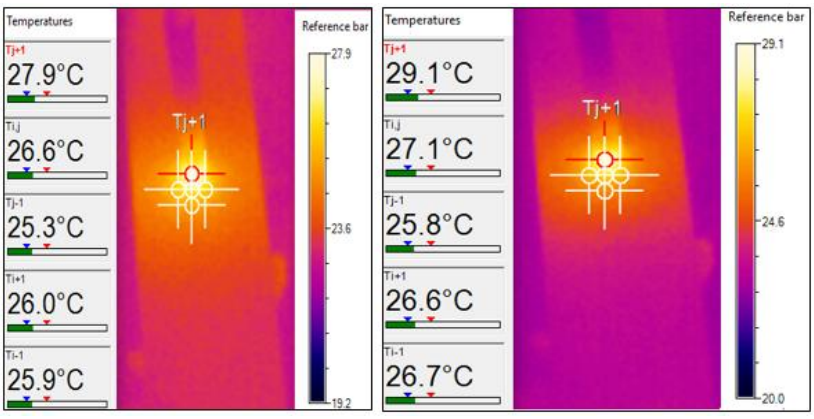


*(a)* *(b)*

**Figure 4:** IR thermal images for shaker forcing frequency *(a) 20 Hz and (b) 50 Hz.*

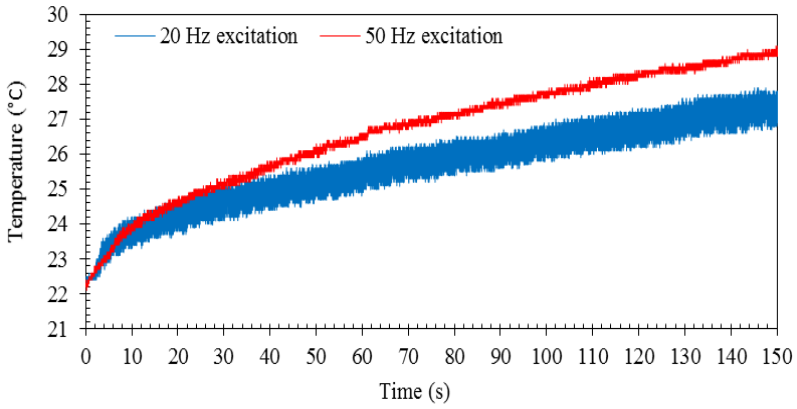


**Figure 5:** Frictional temperature time-domain waveform.

The MATLAB FFT algorithm developed in section 2.1 was utilised to transform the frictional temperature evolution time history (Fig. 5) into the frequency domain as shown in Fig. 6. The vibration frequencies correspond to the longest peak of the spectrum, hence, extracted as 20.0059 *Hz* (Fig. 6a) and 50.0015 *Hz* (Fig. 6b) for the beam forcing frequencies of 20.0 *Hz* and 50.0 *Hz*, respectively.

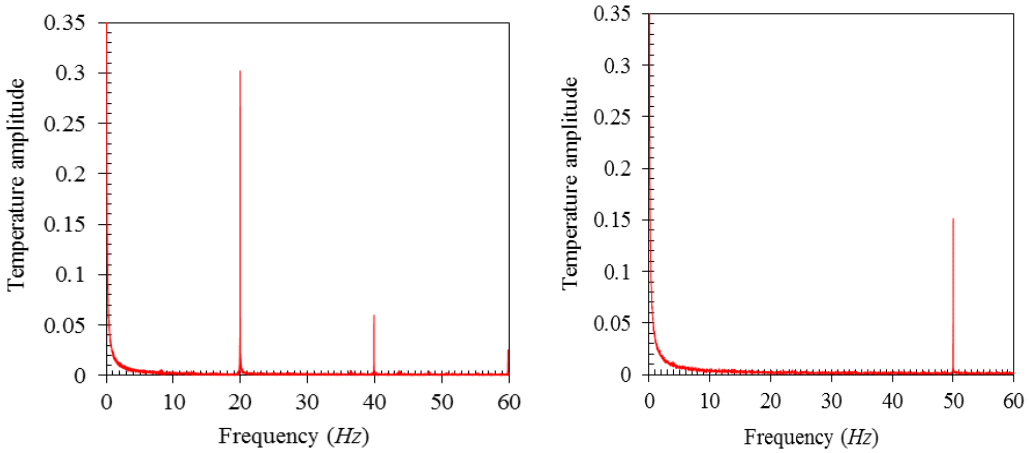


*(a)* *(b)*

**Figure 6:** FFT of temperature evolution *(a)* at 20.0 *Hz and (b) at* 50.0 *Hz.*

The interface contact resultant force, $F_{CR,}$ was computed based on the representation given in Fig. 7.

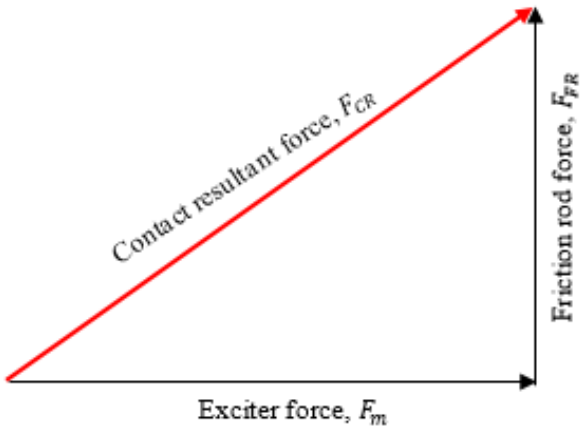


**Figure 7:** Beam-friction rod interface force components.

where, $F_{CR} = \sqrt{\left({F_m}^2 + {F_{FRP}}^2\right)}$, $F_m$ is the maximum exciter force and $P_{FRP}$ is the friction rod pre-load force.

Therefore, interface frictional force corresponding to the excitation frequencies of 20.0 *Hz* and 50.0 *Hz* evaluated as 5.974 *N* and 6.826 *N*, respectively. The beam displacements were analysed using the finite element approach proposed in section 2.2 in conjunction with the interface temperature distribution in Fig. 4. In the case of 20.0 *Hz* (Fig. 4a), the finite nodal temperature using equation 3 along *X* and *Y* directions were -1.3 °C/$mm^2$ and 0.00 °C/$mm^2$, respectively. From equation 7, the IRT predicted displacement obtained as 2.239 *mm*. Similarly, in the case of 50.0 *Hz* (Fig. 4b), the finite nodal temperature along *X* and *Y* directions were -0.9 °C/$mm^2$ and 0.7 °C/$mm^2$, respectively; while the displacement using equation 7 was obtained as 0.877 *mm*. The greater displacement observed at 20.00 *Hz* compared to at 50.0 *Hz* justifies the larger temperature range variation for the former than the latter as depicted in Fig. 5.

On the other hand, the frequency responses presented in Fig. 8 acquired using the described accelerometer, extracted the beam vibration frequencies as 20.0196 *Hz* and 50.049 *Hz* for 20.0 *Hz* and 50.0 *Hz* forcing frequencies, respectively. Interestingly, these compared quite well with those measured using IRT approach with relative errors being 0.07 % and 0.09 % for the former and latter, respectively. Furthermore, the beam displacement spatial statistics was as shown in Table 3 with mean being 2.108 *mm* and 0.912 *mm* for the forcing frequencies of 20.0 *Hz* and 50.0 *Hz*, respectively; the relative errors being 5.85 % and 3.98 % for the former and latter. These errors were attributed to the partly location of accelerometer towards the beam fixed end and use of the coefficient of friction as well as convective heat losses from the literature that may not be the real values as per the experimental setup.

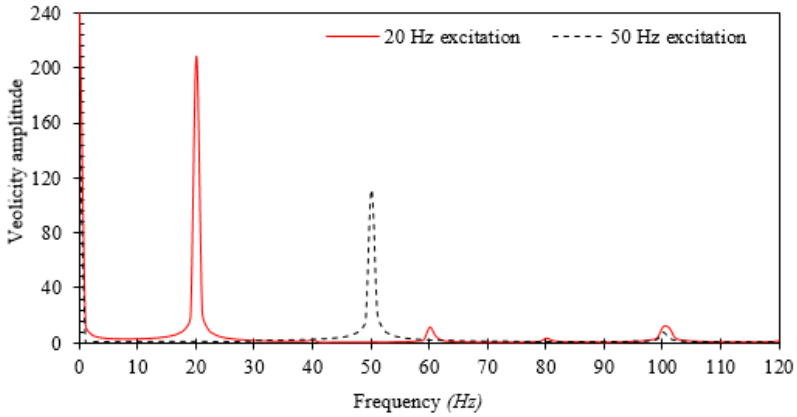


**Figure 8:** Beam FFT of velocity response.

**Table 3:** Accelerometer measured displacement statistics.

| | Beam displacement *(mm)* | |
|---|---|---|
| Description | 20.0 *Hz* forcing frequency | 50.0 *Hz* forcing frequency |
| Mean | 2.108 | 0.912 |
| Max | 6.303 | 2.002 |
| Min | 0.010 | 0.025 |
| Range | 6.293 | 1.977 |
| Std. deviation | 2.015 | 0.619 |

## V. Conclusion

In this paper, the adequacy of monitoring the mechanical structural vibration behaviour in terms of frequency and displacement based on a simple cantilever beam coupled with a friction interface using IRT has been examined practically. The good agreement exhibited by IRT and accelerometer measured dynamic parameters was an evidence of the suitability of the developed methodology. Importantly, this technique finds its strong application in online structural vibration frequency prediction as opposed to displacement since the coefficient of friction cannot be obtained quickly. Moreover, the frictional thermal distribution showed to be non-linear in nature and the equations of finite difference grid can be used to compute the structural displacement from the thermal imager. The findings of this study have a great significance to the mechanical and aerospace engineering communities for the effective structural health monitoring of dynamic structures online using infrared thermography, thus, reducing the downtime and maintenance cost, leading to increased efficiency.

## Acknowledgements

The authors greatly appreciate the support of Eskom Power Plant Engineering Institute (Republic of South Africa), University of Pretoria and Tshwane University of Technology for funding this research.

## References

[1] F. Wei, Q. Pizhong, Vibration-based Damage Identification Methods: A Review and Comparative Study, Structural Health Monitoring 10(1), 2010, 83-111.
[2] N.K. Mukhopadhyay , S.G. Chowdhury, G. Das, I. Chattoraj, S.K. Das, D.K. Bhattacharya, An investigation of the failure of low pressure steam turbine blades, Engineering failure analysis 5(3), 1998, 181-193.
[3] S.E. Moussavi Torshizi, S.M. Yadavar Nikravesh, A. Jahangiri, Failure analysis of gas turbine generator cooling fan blades, Engineering Failure Analysis 16(5), 2009, 1686-1695.
[4] T.T.H. Le, N. Point, P. Argoul, G. Cumunel, Structural changes assessment in axial stressed beams through frequencies variation, International Journal of Mechanical Sciences 110 2016, 41-52.
[5] S.J. Rao, Turbo-machine blade vibration (first edition), New Delhi: New age international publishers 1991, 7-20.
[6] B.O. Al-Bedoor, Discussion of the available methods for blade vibration measurement, In: ASME 2002 Pressure Vessels and Piping Conference. Vancouver, BC: Canada. 1561 2002, 53-61.
[7] P. Castellini, M. Martarelli, E.P. Tomasini, Laser Doppler Vibrometry: Development of advanced solutions answering to technology's needs, Mechanical systems and signal processing 20 2006, 1265-1285.
[8] N. Brock, J. Hayes, B. Kimbrough, J. Millerd, M. North-Morris, M. Novak, C.J. Wyan, Dynamic Interferometry, *In:* Proceedings of SPIE 5875 2005.
[9] J. Renshaw, J.C. Chen, S.D. Holland, T.R. Bruce, The sources of heat generation in vibrothermography, NDT & E International 44(8), 2011, 736-739.
[10] F. Mabrouki, M. Thomas, M. Genest, A. Fahr, Frictional heating model for efficient use of vibrothermography, NDT & E International 42(5), 2009, 345-352.
[11] B.B. Lahiri, S. Bagavathiappan, C. C. Soumya, V. Mahendran, V.P.M. Pillai, J.P. J., T. Jayakumar, Infrared thermography based defect detection in ferromagnetic specimens using a low frequency alternating magnetic field, Infrared Physics & Technology 64 2014, 125-133.
[12] R. Montanini, F. Freni, Correlation between vibrational mode shapes and viscoelastic heat generation in vibrothermography, Ndt & E International 58 2013, 43-48.
[13] M. Singh, G. Lucas, Blade design & analysis for steam turbines, The McGraw-Hill Companies: United States of America 2011, 20-60.
[14] A. Guran, F. Pfeiffer, K. Popp, Dynamics with friction modelling, analysis and experiments, World scientific: Singapore 2001
[15] G. Straffelini, Friction and Wear: *Methologies for design and control*, Springer: Trento 2015, 21-58.
[16] A.D. Dimarogonas, S.A. Paipetis, T.G. Chondros, Analytical Methods in Rotor Dynamics (second edition) New York London: Springer Dordrecht Heidelberg: 2013.
[17] S. Bagavathiappan, B.B. Lahiri, T. Saravanan, J. Philip, T. Jayakumar, Infrared thermography for condition monitoring – A review, Infrared Physics & Technology 60 2013, 35-55.
[18] A.D. Dimarogonas, N.B. Syrimbeis, Thermal signatures of vibrating rectangular plates, Journal of Sound and Vibration 157(3), 1992, 467-476.
[19] D. Thorby, Structural dynamics and vibration in practice: An engineering handbook, London: Elsevier Science 2008.
[20] R.K. Rajput, Heat and Mass Transfer, S. Chard & Company Ltd 2006, 30-40.
[21] S.F. Miller, A.J. Shih, Thermo-Mechanical Finite Element Modeling of the Friction Drilling Process, Journal of manufacturing science and engineering 129 2007, 531-538.
[22] C.F. Beards, Structural vibration: Analysis and damping, London: Elsevier Science 2003, 200-210.
[23] W.P. Sanders, Turbine steam path engineering for operations and maintenance staff (first edition), Richmond Hill, Ontario: Canada 1996, 236-239.
[24] C.V. Madhusudana, Thermal conductance of cylindrical joints, International Journal of Heat and Mass Transfer 42 1999, 1273-1287.
[25] J.T. Oden, J.A. Martins, Models and computational methods for dynamic friction phenomena, Computer methods in applied mechanics and engineering 52 1985, 527-634.